PCCP

Accepted Manuscript

ROYAL SOCIETY OF CHEMISTRY

www.rsc.org/pccp

Journal Name

RSCPublishing

ARTICLE

Platinum/Carbide Interactions: Core-Shells for Catalytic use

Cite this: DOI: 10.1039/xoxxoooooox

J.L.R.Yates[a] , G.H. Spikes[b] and G. Jones[a,c*]

Received ooth January 2012,
Accepted ooth January 2012

DOI: 10.1039/xoxxoooooox

www.rsc.org/

Abstract

A selection of carbides (TiC, NbC, TaC, WC and SiC) have been studied using Density Functional Theory. Their calculated adsorption characteristics towards Pt overlayers are presented with a view to the use of the carbides as core-shell components. WC hcp and SiC are observed to support Pt overlayers on all surfaces making them promising candidates for full Pt encapsulation. Pt adsorption on fcc(111) carbide surfaces is observed to take place with the transition metal surface resonances (TMSRs) playing a key role whilst fcc(100) are universally unfavourable towards Pt adsorption. The effect of the carbide supports on oxygen binding on the Pt overlayer is also considered and discussed in relation to the oxygen reduction reaction (ORR). The oxygen adsorption study revealed several Pt/WC surfaces which exhibit reduced oxygen adsorption energies, suggesting they should promote or maintain ORR activity with respect to nanoparticulate Pt catalysts.

Introduction

The need for clean, sustainable sources of energy for transportation has spurred on research in fuel cells over recent years. Of particular interest has been the hydrogen fuel cell as a replacement for diesel engines.[1] One of the major barriers to large scale commercialization of hydrogen fuel cells for cars is the high cost of platinum which is the main constituent of the membrane electrode assembly catalyst.[2,3] The US Department of Energy targets for vehicular fuel cells require a reduction in Pt loading to 0.125g/kW with an increased cathode mass activity of 0.44 A/mgPt.[4]

One strategy to achieve the DOE targets is via the use of core-shell nanoparticles where a stable, inexpensive core is encased by an atomically thin layer of Pt, resulting in reduced Pt usage and increased Pt availability. Bi-metallic systems and alloyed cores using platinum group metals (PGMs) and transition metals (TMs) have been studied both experimentally[5,6,7] and theoretically[8,9] highlighting Pt skinned Pt_3Ni and Pt_3Y alloys as possible oxygen reduction reaction (ORR) catalysts with improved activity. Other non-metallic materials have also been considered as supports for Pt such as metal oxides, nitrides and carbides.[10,11,12] The work presented herein will consider the use of transition metal carbides as core materials.[13,14]

Carbide materials are particularly interesting for fuel cell applications as they exhibit high thermal stability, excellent conductivity (both electrical and thermal) and are corrosion resistant.[15,16] It has also been noted in the past that hcp WC has 'Pt-like' electronic structure in the region of the Fermi level (E_f) and exhibits some innate catalytic ability,[17] although the extent of this Pt-likeness is limited.[18] Theoretical calculations by Hsu, Esposito and co-workers have previously shown that WC(0001) with a Pt overlayer produced Pt(111)-like binding energies for reagent molecules such as oxygen and hydrogen.[19,20] In the case of Pt/WC(0001), a -0.04eV deviation from the Pt(111) O binding energy was calculated suggesting that the catalytic activity of the Pt in such systems should largely be maintained.

Significant success in understanding molecular adsorption interactions at TM surfaces has been achieved through the d-band centre model.[21] This model correlates the surface electronic structure with reagent binding energies, which in-turn determines the catalytic activity of a given TM. The use of core materials can alter the d-band centre of the Pt ML via lattice strain,[22] and ligand effects,[23] raising the possibility of tuning catalysts for specific reactions. These alterations are noted in the current work and discussed in terms of the modulation of the electronic structure. In the adsorption of atoms on TM carbides however, deviation from the d-band model has been noted.[24] A modified Newns-Anderson type model for molecular and atomic adsorption at carbide and nitride surfaces has been proposed which considers adsorption interactions with surface resonances.[25,26] We test this modified model with regard to the adsorption of Pt overlayers on to the carbides.

Journal Name RSCPublishing

ARTICLE

Table 1 Bulk material properties including metal electronegativity (χ) in the Pauling scale,[27] net charges on the metal atom, the gap between the valence and conduction d-band centres (Δ) and the d-band centre (E_d). For SiC Δ was calculated from the total DOS band centres.

Material	Calculated Lattice Parameter (Å)	Literature Lattice Parameter (Å)	Metal χ	Net Bader Charge (e)	Net Mulliken Charge (e)	Δ (eV)	E_d (eV)
TiC	4.37	4.33[a](4.33)[f]	1.5	1.64	0.68	5.68	0.12
NbC	4.50	4.47[b](4.49)[f]	1.6	1.66	0.7	6.50	-1.38
TaC	4.57	4.46[b](4.48)[f]	1.5	1.76	0.74	6.78	-0.44
WC (hcp)	2.93, 2.85	2.91, 2.84[c](2.92,2.84)[g]	1.7	1.40	0.6	8.45	0.54
WC (fcc)	4.39	*(4.38)[f]	1.7	1.64	0.69	6.80	-2.29
SiC-β	4.37	4.36[d](4.39)[h]	1.9	3.03	1.24	10.02	-
Pt	4.01	3.92[e](4.02)[i]	2.2	-		-	-2.46

*experimental data unavailable. References: a[28], b[29], c[30], d[31], e[32], Theoretical values in brackets: f[33], g[34], h[35],i[36]

The aim of the work presented herein is to identify carbides suitable for use in fuel cell applications. In order to do this we seek firstly to understand the Pt/carbide adsorption trends with respect to the electronic structure, following which, we assess the effect of the carbide on the Pt overlayer and finally identify systems which may maintain or enhance the ORR via oxygen adsorption calculations.

Results and discussion

Bulk Carbides

Six carbides were selected for this work; the face-centred cubic (fcc) forms of TiC, TaC, NbC and WC, hexagonal close-packed (hcp) WC and zinc blende SiC known as β or 3C-SiC[37] as a non-transition metal comparison. This group of carbides was chosen to provide a comparison of trends resulting from different elements and the geometric influence of crystal structure on Pt adsorption. Carbides formed from TMs in groups 4, 5, and 6 are interstitial compounds in which the smaller C atoms fit into the closed packed metal lattice, SiC however is a covalent carbide due to the smaller difference in electronegativity between its constituent elements. The TM carbides are known to exhibit varying degrees of covalent, ionic and metallic bonding character.[38] This is illustrated in our calculations through topological analysis of the electron density[39] and analysis of the density of states (DOS). The d-band centres of the carbide materials are taken as the mean energy of the TM d-band. The bulk carbides have been previously described by Johansson *et al*, Vojvodic *et al* and Viñes *et al.* [15,33,40] Readers are directed there for a more comprehensive treatment of the trends mentioned herein.

Table 1 displays the bulk lattice parameters and charge density distribution of the carbides studied in this work. The calculated lattice parameters were found to be in good agreement with the published experimental data and theoretical values calculated using GGA functionals. Topological analysis of the electron density reveals charge being transferred from the metal to the carbon in each of the materials, due to the higher electronegativity of carbon (2.55 on the Pauling scale). For the early transition metals, charge transfer is observed to increase down the group as the electronegativities of the metals decrease. Across the period from Ta to W the charge transfer decreases. A difference in charge transfer is also noted between the two crystal structures of WC suggesting that the hcp form of WC is more covalent than the fcc. The covalently bonded SiC is the exception here, exhibiting double the charge transfer indicated in the other compounds. The same trends were also observed using an alternative charge partitioning method (Mulliken analysis[41]) which adds credence to these results.

Trends in the electronic structure of the fcc carbides can be seen in the DOS plots included in the supplementary material, however those for hcp and fcc WC are displayed in figure 1. Unlike in the fcc TM carbides, hcp WC has much broader bands suggesting more electron delocalisation and supporting the assertion of more covalent bond character indicated by the Bader analysis. The smaller gap between the valence and conduction band centres (Δ) observed for the fcc WC indicates it's relative instability compared to hcp WC due to unfavourable filling of anti-bonding orbitals in agreement with Li *et al.*[42]

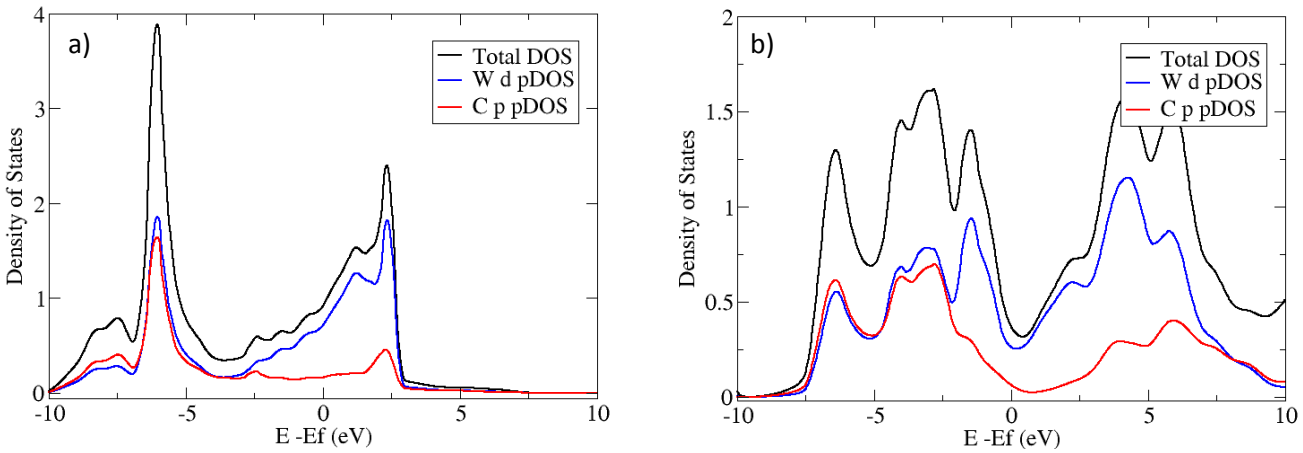

Figure 1 Total and projected Density of States (DOS) around the Fermi level (E_f) a)) fcc WC and b) hcp WC

SiC also differs from the TM carbides as it is a semiconductor with a calculated band gap of 1.42 eV. This is significantly less than the literature value of 2.39eV.[43] The discrepancy is due to the oft-cited self- interaction error due to the approximate nature of the GGA exchange correlation functionals, which can lead to band gaps being underestimated.[44]

Carbide surfaces

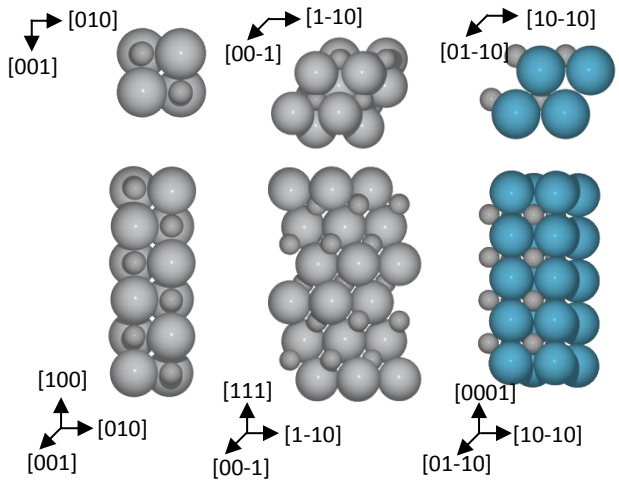

Figure 2 From left to right, schematic representations of fcc {100}, {111} and hcp {0001} surfaces top and side view

After optimisation of the bulk properties, the (100) and (111) surfaces for the cubic systems and additionally the (0001) surface for the hcp system, were cut using the Atomic Simulation Environment.[45] Slab depths were converged to give surface area energies consistent to 0.02 eV and a vacuum distance of 10Å was included to prevent interference between repeated images under periodic boundary conditions. For fcc-(111) surfaces a minimum of five carbide layers were used and for fcc-(100) a minimum of six layers with the back 2 layers in each case constrained to bulk lattice positions. Symmetrical double sided slabs were used for the calculation of the surface energies to prevent creation of a surface dipole. Both carbon and metal rich surfaces are accessible experimentally, therefore both are studied herein.

Surface energies (E_{surf}) were calculated using equation 1.

$$E_{surface} = \frac{E_{system} - (nE_{bulk} + nE_C + nE_X)}{2A} \quad (1)$$

Where E_{system} is the energy of the calculated surface slab, n is the number of units within the system, E_{bulk} is the energy of a TMC unit in the bulk, E_c is the calculated energy of a unit of graphene,[†] E_X is the calculated energy of a unit of bulk metal or Si and A is the surface area.

It is seen in Table 2, that the fcc-(100) surface is the most stable for the fcc carbides. This observation can be rationalised via the bond-breaking model due to the strength of the M-C bonds and the number of these bonds broken to create the (100) and (111) surfaces (1 and 3 respectively).[46] In cases where carbon terminated as well as metal terminated surfaces have been calculated, the carbon terminated surfaces are significantly less stable than their metal counterparts.

Surface relaxations are known to significantly impact carbide surface energies and as such were included to prevent serious error in the calculated energy values.[40] Whilst there are a number of surface reconstructions known for SiC,[47] herein we only considered idealised terminations to facilitate comparison with TM carbide structures. Typically the TM carbides experience intra- and interlayer contraction and expansion producing ripples in the top most layers of the materials.

Table 2. Carbide surface energies, % change in intra- and interlayer distances and surface iconicity (charge relative to the neutral atom). Intralayer distances for (100) show TM-C values, see supplementary material.

Surface	Energy (Jm^{-2})	Intralayer change (%)	Interlayer change (%)	TM charge	C charge
TiC(100)	1.48	-2.1	-0.7	1.64	-1.58
NbC(100)	1.12	-7.7	-4.4	1.61	-1.59
TaC(100)	1.19	-4.8	-1.2	1.66	-1.61
WC(10$\bar{1}\bar{1}$0)hcp	4.16	12.7	0.5	0.92	-1.40
WC(100)fcc	0.51	-6.2	-7.5	1.53	-1.49
SiC(100)	2.64	-2	0.5	1.53	-3.08
CSi(100)	3.24	-12.9	-7	3.10	-1.69
Pt(100)	1.72	-	-2.1	-	-
TiC(111)	3.90	-16.1	-2.7	1.10	-1.81
NbC(111)	1.28	-15.4	-4.8	0.94	-1.72
TaC(111)	1.64	-11.7	-5.4	0.98	-1.81
WC(11$\bar{2}\bar{2}$0)hcp	4.39	0.7	0.2	-	-
WC(0001)hcp	3.17	-4.5	-1.4	0.67	-1.34
WC(111)fcc	2.07	-20.3	-8.1	0.86	-1.63
CW(111)fcc	3.03	-24.3	-6	1.70	-0.98
SiC(111)	2.57	-0.4	2	0.77	-3.1
CSi(111)	4.09	-12.8	-12.9	2.98	-0.84
Pt(111)	1.40	-	1.1	-	-

As seen in Table 2, the most significant ripple effects are seen in the fcc-(111) surfaces, which experience contractions of 10-25% in excellent agreement with literature values.[26] A less significant rumpling occurs for the fcc-(100) surfaces in agreement with Viñes.[40] For materials where C and TM terminated surfaces were calculated, the C terminations exhibited a much greater degree of contraction as the C atoms were drawn towards the bulk to minimize the surface energy. In the case of hcp WC, less contraction is noted for the hcp-(0001) surface[48] than the fcc-(111) surfaces and the hcp-(10$\bar{1}$0) surface is observed to expand in to the vacuum layer. The SiC surfaces exhibit smaller variations from the bulk than the fcc surfaces, although greater contraction of the C terminated surfaces is still observed. First layer contractions are much greater than those in subsequent layers and bulk layer values were restored within 3 bilayers. For the fcc-(100) surfaces where C and TM were present at the surface it was noted that TM atoms were drawn into the surface whilst C atoms moved away from the bulk.

Variation in charge transfer is noted between the bulk and the top-most atoms at the surface. Bulk charge values were also restored across our subset of studied carbides upon reaching the third bilayer. Loss of electrons from the TM element to the C element was noted particularly for the fcc-(111) surface bilayer and the degree of change was similar whichever termination was present. For the fcc carbides, the fcc-(100) first layer showed little charge alteration as both carbon and metal atoms are present in each layer. The SiC surfaces exhibited significant electron loss at the surface (for both terminations) which was countered by a gain in charge density in the second layer. The surface charge density descriptions of TM terminated fcc-(111) carbides shown here are in good agreement with the work of Vojvodic.[26]

Surface specific electronic structure contributions of the carbides were found upon subtracting the bulk DOS from the The positive peaks represent surface resonances (SR). For fcc-(111) surfaces at or around E_f a resonance with TM nature is observed, whilst below E_f in the valence band a mixed TM-C resonance is found and lower still in energy, a C resonance is present. As observed in the bulk DOS, with increased d-band filling the valence and conduction bands of the surface shift down in energy, this observation is also true of the TMSRs. The amplitude of the TMSR is observed to decrease and the bandwidth broaden as you travel down the TMs. TMSRs are also noted for hcp WC in a similar region to TiC(111) and for SiC a Si resonance is observed just below E_f.

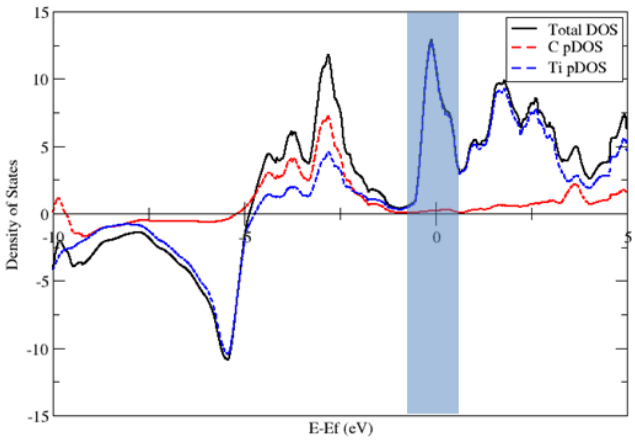

Figure 3 Difference Density of States plot showing the surface specific electronic structure for TiC(111), TMSR highlighted in blue

For the fcc-(100) surfaces, the difference DOS is dominated by unfilled TM bands above E_f which are shifted lower in energy as the d-band is filled. Below E_f there are small TM maxima between -5 and -2 eV however the DOS is dominated by the filled C p-orbitals. A TMSR was observed at E_f for hcp WC however for SiC no significant resonance was noted below E_f. It has previously been shown that the mean energy of these TMSRs (E_{TMSR}) can be used to explain atomic and molecular adsorption on the TMC fcc-(111) surfaces.[49] In this study we considered the effect of TMSRs upon Pt ML adsorption.

Pt Monolayer Adsorption

Pt site preference was tested with single and multiple adsorptions of Pt atoms on the possible carbide adsorption sites. For fcc-(100) surfaces Pt atop the surface C atom was favoured with the exception of SiC(100) where a Si bridging site was observed. For fcc-(111) surfaces the 3-fold hollow sites were of very similar energies, with the tetrahedral site proving the most

favourable. Pt overlayers were constructed through sequential addition of Pt to the preferred site. Coverages from 0.5-3 monolayers (ML) of Pt were studied, focusing on the strength of adsorption and variation of the electronic structure, in particular the d-band centre (or average energy of the d-electrons E_d) of the Pt atoms. Adsorption energies were calculated using equation 2.

$$E_{ads} = \frac{E_{Slab+Pt} - (E_{slab} + nE_{Pt\,bulk})}{nPt} \quad (2)$$

Generally the resulting Pt overlayers are reminiscent of the symmetry of the surfaces they adsorb to, *i.e.* fcc carbide (100) surfaces produce fcc-(100) like Pt layers, hcp WC(0001) surface yields an fcc-(111) like Pt surface. The hcp carbide's (11-20) surface results in a stepped Pt layer with the first layer having a coverage of 0.5, this is shown in the supplementary material figure 3.

Figure 4 displays the energetics of the Pt monolayer adsorption on to the WC, TiC and SiC surfaces. In the case of hcp WC and SiC, each of the constructed surfaces exhibit favourable Pt adhesion suggesting total encapsulation of nanoparticulate carbide may be possible. As would be expected, the differential adsorption energy converges towards the bulk Pt value as the overlayer thickness increases. For these materials, the order of surface preference for monolayer adsorption is:

C terminated > (100) > (111)

which follows the trends of the surface energies recorded previously (in table 2). It is generally observed that less stable surfaces prove more reactive for Pt adsorption. In the case of fcc TiC and WC, the (100) surfaces proved unfavourable towards Pt adsorption while the (111) surfaces were preferentially coated again following surface energy trends.

Thus SiC and hcp WC are expected to be promising core materials as Pt adsorption on the most common surfaces is strongly favoured. For fcc TM carbides the lack of Pt adhesion to the fcc-(100) surfaces is problematic when considering the carbides as core-shell components. The (100) surface would provide a significant fraction of the nanoparticulate carbide surface facets and full encapsulation of the carbide would be needed to prevent core corrosion and Pt dissolution. The introduction of other layers to buffer the core or provide an anchor to the Pt is a possible solution to this problem and within our group metallic tie layers have been trialled for this purpose with promising results.[50]

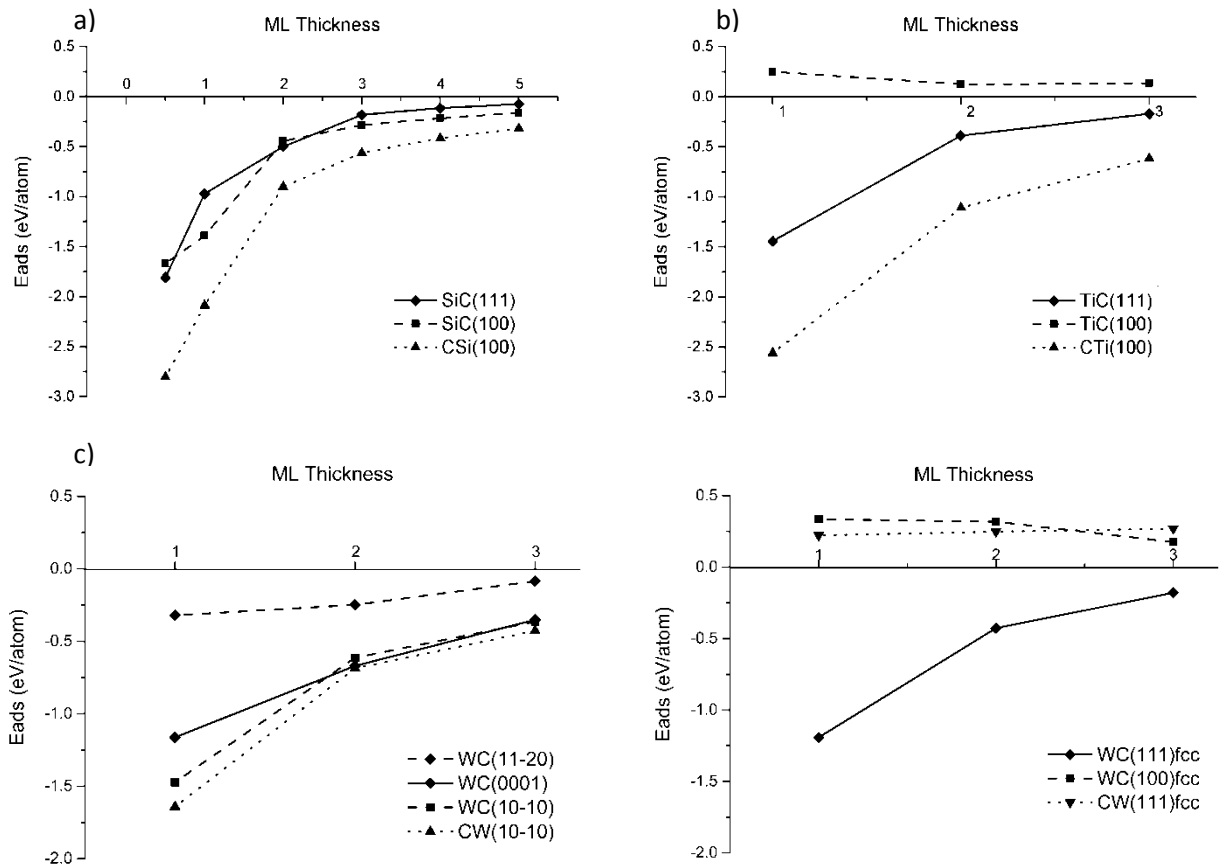

Figure 4 Pt overlayer adsorption trends a)SiC, b)TiC, c) hcp WC, and d) fcc WC

Journal Name RSCPublishing

ARTICLE

Having considered the energetics, we now move to consider an electronic explanation of the Pt adsorption behaviour of the carbides. For the fcc carbides, charge transfer onto the Pt was observed for all TM terminated surfaces. In the case of the fcc-(100) surfaces, the electron density is observed to be mainly from the C atoms whereas for the fcc-(111) surfaces it is from the TM surface layer. The degree of charge transfer observed was greater for the fcc-(111) than for the fcc-(100) ranging from -0.6 to -0.47 and -0.3 to -0.15 electrons respectively. For the C terminated surfaces, density moved from the Pt overlayer into the C surface and subsurface layers leaving a +0.12-0.14 charge on the overlayer in each case. The degree of charge transfer was similar for the hcp WC surfaces, with the (0001) surface acting like an fcc-(111) surface. As in the clean surfaces, a much greater degree of charge transfer was noted for SiC with -1.3 and -1.8 electrons being transferred to the Pt atoms on the (100) and (111) surfaced respectively.

Subsequently, correlation between the E_d of the carbide surfaces and the E_{ads} of the Pt was sought. Deviations from the d-band centre model are observed for adsorptions on the TM carbides and can be seen in figure 5a. Here we observe fcc-(100) surfaces with differing E_d produce very similar adsorption energies. If the C terminated fcc-(111) surfaces are considered along with the M terminated, a loose trend can be observed in which increasingly negative E_d results in weakened Pt adsorption as expected, however the fcc WC (111) clearly diverges from this pattern. The hcp WC (0001) does coincide with the fcc-(111) adsorption region although the $(10\bar{1}0)$ surfaces do not act like its fcc-(100) counterparts as previously noted and no correlation between E_d and E_{ads} may be made. The SiC surfaces cannot be included in this analysis as Si is not a TM and so contains no d electrons.

Previously Kitchin *et al.* suggested that incorrect charge partitioning of the carbide may result in overly negative E_d values and highlighted the fact that the introduction of the C in the carbide would have an impact on the TM d-band shape.[24] We conclude that the d-band centre is of limited usefulness in explaining the observed Pt adsorption behaviour.

Difference DOS plots before and after Pt adsorption reveal the depletion of the TMSRs present on each of the (111)-type surfaces indicating that they are involved in the bonding of the Pt (see supplementary material).[26] In figure 5b we can see that as E_{TMSR} becomes increasingly negative the adsorption strength does weaken. However, this trend is much weaker than for reagent adsorptions as the Pt DOS is much broader than that of isolated atoms such as O or H, making the bonding anti-bonding splitting less distinct and so the correlation weaker. For fcc-(100) surfaces band density depletions are noted at the energies where the surface resonances were observed, however the depletions are dominated by C states which coincide with the charge density changes previously discussed. This being the case the E_{TMSR} provides a less adequate description of the Pt adsorption on fcc-(100).

Figure 5 a) Plot of the E_d for clean TM carbide surfaces versus the adsorption energy of 1ML Pt b) Plot of E_{TMSR} versus adsorption energy of 1ML of Pt for TM(111) surfaces

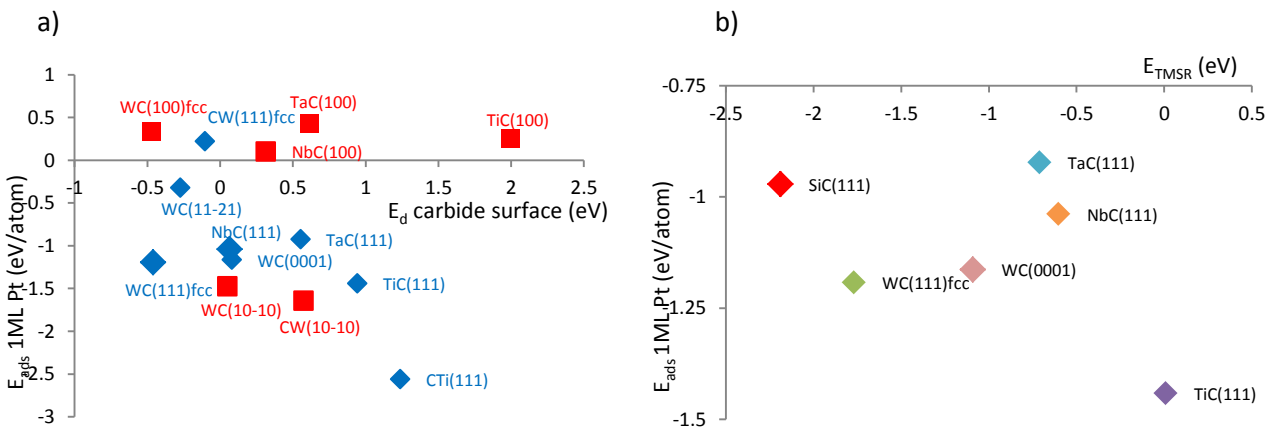

The Pt overlayer E_d are subject to lattice and ligand effects via interaction with the carbide surface. Lattice mismatch between the carbide and the Pt overlayer creates strain in the overlayer and alters the Pt orbital overlap, altering the width of the d-band in the DOS. Heteroatomic bonds formed between the Pt and carbide surface atoms will also result in changes to the bandwidth. In order to maintain the filling of the d-band, the d-band centre is shifted towards or away from E_f.[22] For example, expansion of the Pt lattice parameter reduces Pt-Pt orbital overlap and so narrows the d-band width resulting in E_d moving towards E_f. The effect of the carbide core on the Pt monolayer is exemplified by the DOS plot in Figure 6. The primary Pt layer applied to the surface exhibits a significant negative shift and narrowing of the bandwidth due to the expansion of the lattice and the formation of Pt-Si and Pt-C bonds. As the Pt ML thickness increases, the DOS for the outer layer of Pt in the overlayer becomes more reminiscent of that for the pure Pt; E_d moves back towards E_f and the bandwidth increases. This pattern is repeated for Pt over layers on the other carbides as shown for hcp WC(0001) in the supplementary material. It is important to note that whilst the electronic effect of the carbide will be lessened as the number of Pt layers, N, increases, due to the periodic boundary conditions of the model the lattice parameter miss-match cannot self-heal as has been observed in experiment.[51] This is due to the fact that the unit cell of the overlayered system is constrained to the carbide lattice parameters and a computationally unfeasible cell would be required to capture such effects.

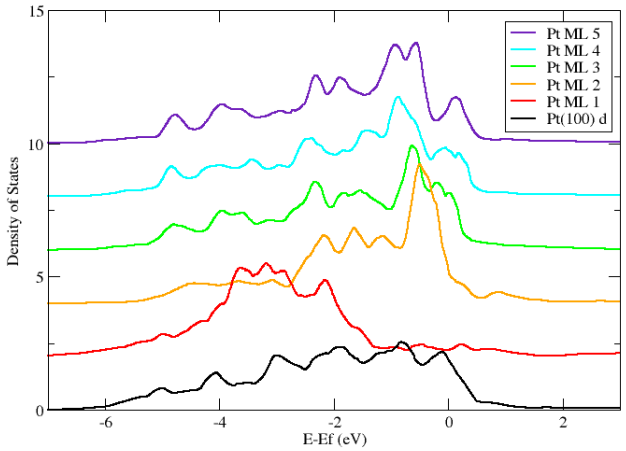

Figure 6 Projected Density of States diagram for the d-band of Pt ML on SiC(100), each ML d-band is offset for clarity

To assess the extent of the geometric effect versus electronic interaction, Pt(100) and Pt(111) surfaces were expanded to the various carbide unit cell sizes and their electronic structures calculated. For the fcc carbides the degree of area mismatch is due to the radius of the metal involved in the structure which varies from +4-30%. It is necessary to note that the more significant mismatches resulted in several of the overlayers being in a transition region between their initial surface type and other surfaces *i.e.* having an intermediate character. In this analysis the Pt overlayers were compared to the pure surfaces most like their construction *i.e.* the Pt-WC(0001) is compared to Pt(111).

In figure 7 the expansion of the Pt lattice parameter is seen to decrease the value of E_d, shifting it closer to the E_f. The supported Pt E_d values are consistently more negative due to the ligand effect exerted by the various carbide centres. For the fcc carbides, Pt monolayers on the C terminated surfaces have more negative E_d values than those on the corresponding TM/Si terminated surface. The C terminated surfaces have an increased DOS at the pseudogap and greater C p-density below E_f which result in greater C p-character in the adsorption orbital overlap and the resultant shift in energy.

Following the deconvolution of the carbide core effects, we observe that overall the carbide surface electronic structure has the most significant impact on the resultant E_d of the Pt ML as a range of E_d are seen with little lattice mismatch variation. For the fcc carbides E_d(100) values are consistently 0.1-0.2eV more positive than E_d(111) values for the same carbide. The C terminated (111) surfaces for TiC and fcc WC do not produce a regular energy difference within the general trend. The Pt/hcp WC E_d are arranged in the same energy order although the energy difference between the $(10\bar{1}0)$ and (0001) surfaces is greater at 0.25eV. The hcp WC results exhibit different behaviour with regards to area mismatch. Increased unit cell area results in increasingly negative E_d values with the symmetry of the surface aiding Pt d W d-orbital overlap to overcome the lattice expansion effect.

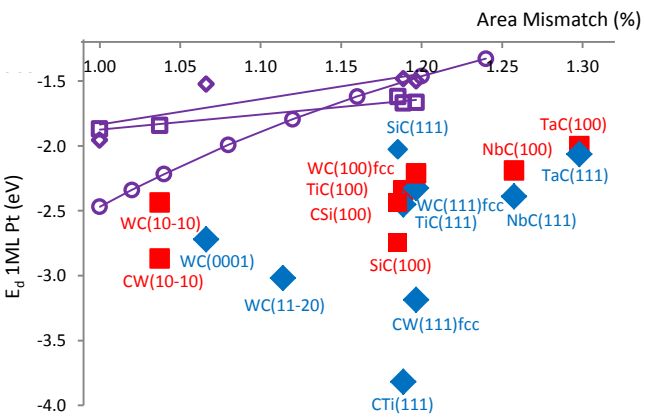

Figure 7 Plot of area mismatch vs E_d for carbide supported Pt. Expanded Pt model is represented by open markers ◊ Pt(111), O Pt bulk and □ Pt(100).

The Pt/SiC surfaces exhibit the opposite trend in surface energy ordering with the Pt/SiC(100) system having a less negative E_d than Pt/SiC(111). The interaction of the Pt with the SiC(100) surface is dominated by C p-states whilst that with the SiC(111) surface has more Si p-character due to the termination of the surface. DOS analysis shows the C states in the SiC(100) surface being further in energy from E_f than the filled Si bands in the SiC(111) and a further negative shift of the total Pt/SiC(100) DOS upon Pt adsorption gives rise to the more negative E_d value.

Activity of Pt Monolayers

Whilst the E_d and E_{TMSR} models do not allow for quantitative prediction of Pt adsorption behaviour, they may still be useful in describing the subsequent adsorption behaviour of the Pt/carbide system. Upon adsorption of a reactant molecule, the position of the anti-bonding states will be related to the d-band centre; a very negative d-band centre may result in the anti-bonding orbitals extending below E_f and being filled weakening the bond. Thus, expansion of the lattice and the shift of the d-band towards E_f should result in stronger bonding interactions.

It is well known that on the transition metals scaling relationships exist between the adsorption energies of O, OH and OHH[52] and subsequent work has proven the extension of these relationships on to carbide and oxide surfaces.[53] This being the case, the O adsorption energy can be used as an indicator of a surfaces' reactivity.[54] Having shown that a Pt ML can be formed on carbide surfaces and gives a resultant shift in the Pt d-band centre; the effect of the carbide core upon the adsorption of atomic O on the Pt overlayer was investigated. This adsorbate is a key intermediate in the ORR and it has previously been shown that by reducing the adsorption energy for O*, where * denotes an adsorbed species, (and thus via scaling relations that of *OH and *OHH) an enhancement of activity would be possible with regard to pure Pt.[9]

As before all high symmetry adsorption sites on the Pt overlayers were trialled with the preferred site being used to place the adsorbate on to the N>1 systems. For the (100) surfaces the bridging site was preferred as on the pure Pt reference whereas for the (111) N=1 surfaces the tetrahedral 3-fold site was slightly favoured over the octahedral. For N>1 it was found that the octahedral site became preferred as on the pure Pt(111).

The relative adsorption energies for the O on the 1 ML Pt overlayer systems can be seen in figure 8. Pt/hcp WC surfaces are found to produce adsorption energies which are less than or similar to those on pure Pt. In the work of Hsu *et al*, a 3x3 unit cell was used, presenting the low coverage scenario for O adsorption.[19] Our calculated difference in adsorption energy for ¼ coverage on the WC(0001) surface was -0.02 eV/atom which is in excellent agreement. This validates our present model using 2x2 (111) slabs as the adsorption results were within the range of error for DFT. It is however noted that for hcp WC, the $(11\bar{2}0)$ surface gives a much stronger O adsorption than Pt which would be unfavourable for the ORR. Given the clean surface energies presented previously the hcp-(0001) surface is likely to be more prevalent in the initial carbide suggesting that hcp WC may still be a suitable core material. The CTi(111) surface also has an O adsorption smaller than that on pure Pt, however the other TiC surfaces bind O more strongly and as these surfaces would be more prevalent in the carbide nanoparticles due to their relative stability, overall TiC would be a less suitable core for the ORR reaction.

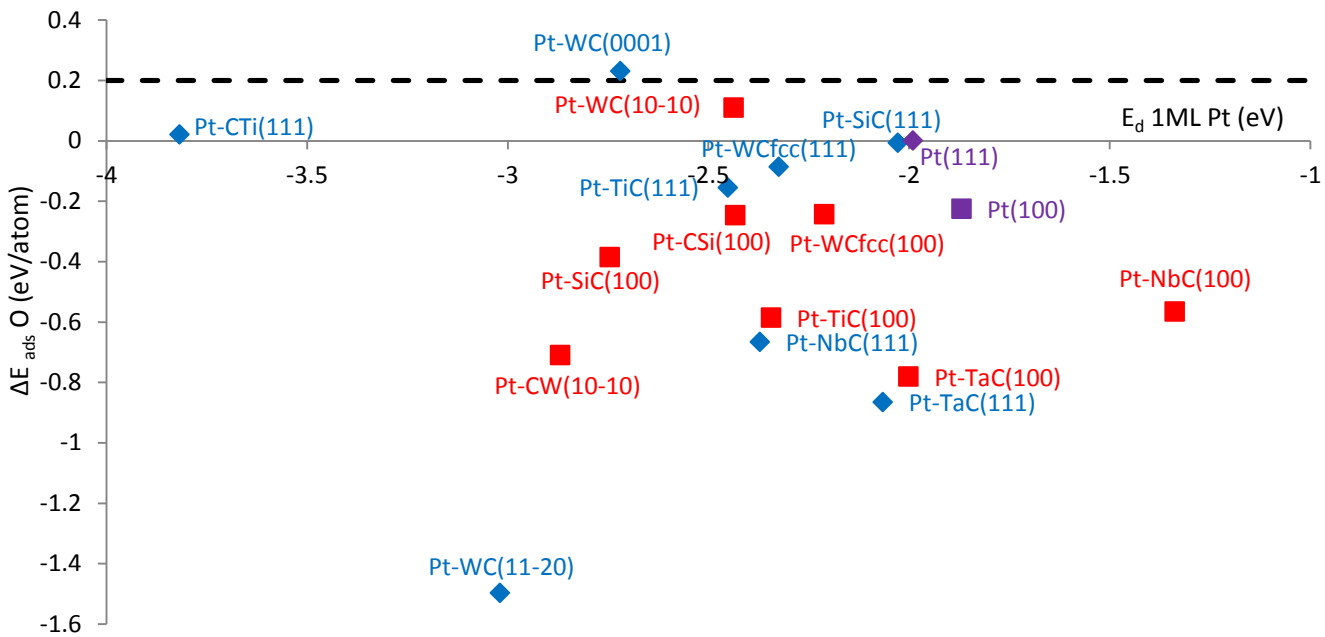

Figure 8 Relative adsorption energies of atomic oxygen on Pt/carbide surfaces at a coverage of 0.5 ML, all values are relative to the most stable O adsorption on Pt(111) Line at 0.2 eV signifies optimum Δ E ads O for ORR.[8]

Theoretical Method

Calculations were carried out using density functional theory as implemented in the planewave code CASTEP.[55] Ultrasoft pseudopotentials[56] were used throughout and the exchange-correlation included using the generalized gradient approximation[57] in the RPBE functional.[58] Bulk calculations were conducted with a Monkhorst-Pack grid [59]of 10x10x10 k-points at an energy cut off of 340eV. Topological analysis of the charge density was carried out using the Bader approach[39] via the Topology code[60] and projected density of states calculations were conducted using LinDOS.[61] Subsequently, 2x2 unit cells were used for the (111) and (0001) surfaces and 1x1 for the (100) surfaces with a Monkhorst- Pack grid of 5x5x1 k-points in each case.

Conclusions

This work has taken a set of bulk carbide materials and studied the interaction of various model surfaces with Pt, the aim being to identify suitable core materials for use in fuel cell applications. The thermodynamic feasibility of the formation of Pt overlayers on carbides was verified and observations rationalised in terms of the modulation of the carbide and Pt electronic structures. We went on to demonstrate the suitability of Pt/carbide materials for the ORR by investigating the influence of the core on atomic O adsorption at the Pt overlayer surfaces.

Good Pt overlayer binding was identified on fcc-(111) carbide surface and the surfaces of SiC and hcp WC studied herein. The expansion of the Pt overlayers due to the carbide lattice parameters was found to shift the E_d towards the E_f, however the ligand effect produced by the formation of heterobonds to the carbide surfaces was more significant and resulted in E_d which were more negative than pure Pt.

Our surface models were verified in their ability to reproduce O adsorption energies of Hsu *et al.*[19] whilst using a computationally less expensive set up, suggesting that fast screening of the carbides using the current method produces reliable and useful results for the guidance of experimental research. Considering the adsorption of atomic oxygen on the overlayers, hcp and fcc WC were identified as possible cores for the promotion of the ORR, however phase stability would suggest that hcp WC would be most suitable.

Whilst a solution to the unfavourable adsorption of Pt on the fcc-(100) surfaces is necessary to provide protection to the core under harsh fuel cell conditions, we conclude that the carbides do show promise as Pt supports with the ability to tune the reactivity of the TMC(111) surface and that hcp WC/Pt may be a suitable ORR catalyst. Some experimental work has been carried out in the area[62,63,19] prompting further investigation of the stability and activity of these systems under fuel cell conditions.[64]

Acknowledgements

Via our membership of the UK's HPC Materials Chemistry Consortium, which is funded by EPSRC (EP/F067496), this work made use of the facilities of HECToR, the UK's national high-performance computing service, which is provided by UoE HPCx Ltd at the University of Edinburgh, Cray Inc and NAG Ltd, and funded by the Office of Science and Technology through EPSRC's High End Computing Programme. The authors also acknowledge the use of the UCL Legion High Performance Computing Facility (Legion@UCL), and associated support services, in the completion of this work. JY would like to acknowledge the EPSRC and Johnson Matthey for funding. GJ would like to acknowledge the Royal Society for funding an Industrial Fellowship and Prof. De Leeuw and Prof. Catlow for hosting him at UCL.

Notes and references

[a] Department of Chemistry, University College London, 20 Gordon Street, London, WC1H OAJ

[b] Johnson Matthey Technology Centre, Blounts Court, Sonning Common, Berkshire, RG4 9NH

[c] Johnson Matthey Technology Centre- Pretoria, Building 22, CSIR, Meiring Naude Road, Pretoria, 0001, ZA

* gjones@matthey.com

† Graphene was chosen as our standard C state as use of graphite would require the inclusion of Van der Waals interactions and the use of a different functional throughout the work.

Electronic Supplementary Information (ESI) available: a schematic for the relaxation of the carbide surfaces, fractional coordinates for the carbide bulk unit cells, and further difference DOS plots are provided. See DOI: 10.1039/b000000x/

1. Johnson Matthey, *Platin. Met. Rev.*, 2012, **56**, 272–273.

2. H. A. Gasteiger and N. M. Markovic, *Science*, 2009, **324**, 48–9.

3. M. K. Debe, *Nature*, 2012, **486**, 43–51.

4. Department of Energy and Office of Energy Efficiency and Renewable Energy, *Fuel Cell Technologies Office Multi-Year Research, Development and Demonstration Plan*, 2011.

5. J. Zhang, M. B. Vukmirovic, Y. Xu, M. Mavrikakis, and R. R. Adzic, *Angew. Chem. Int. Ed. Engl.*, 2005, **44**, 2132–5.

6. N. M. Markovic, T. J. Schmidt, V. Stamenkovic, and P. N. Ross, *Fuel Cells*, 2001, 105–116.

7. C. Wang, M. Chi, D. Li, D. Strmcnik, D. van der Vliet, G. Wang, V. Komanicky, K.-C. Chang, A. P. Paulikas, D. Tripkovic, J. Pearson, K. L. More, N. M. Markovic, and V. Stamenkovic, *J. Am. Chem. Soc.*, 2011, **133**, 14396–403.

8. J. Greeley, I. E. L. Stephens, A. S. Bondarenko, T. P. Johansson, H. A. Hansen, T. F. Jaramillo, J. Rossmeisl, I. Chorkendorff, and J. K. Nørskov, *Nat. Chem.*, 2009, **1**, 552–6.

9. I. E. L. Stephens, A. S. Bondarenko, U. Grønbjerg, J. Rossmeisl, and I. Chorkendorff, *Energy Environ. Sci.*, 2012, **5**, 6744.

10. Y.-J. Wang, D. P. Wilkinson, and J. Zhang, *Chem. Rev.*, 2011, **111**, 7625–51.

11. Y. Shao, J. Liu, Y. Wang, and Y. Lin, *J. Mater. Chem.*, 2009, **19**, 46.

12. V. Tripković, F. Abild-Pedersen, F. Studt, I. Cerri, T. Nagami, T. Bligaard, and J. Rossmeisl, *ChemCatChem*, 2012, **4**, 228–235.

13. T. G. Kelly and J. G. Chen, *Chem. Soc. Rev.*, 2012, **41**, 8021–34.

14. D. V. Esposito and J. G. Chen, *Energy Environ. Sci.*, 2011, 3900–3912.

15. L. Johansson, *Surf. Sci. Rep.*, 1995, **21**, 177–250.

16. Y. Liu, T. G. Kelly, J. G. Chen, and W. E. Mustain, *ACS Catal.*, 2013, 11184–1194.

17. R. B. Levy and M. Boudart, *Science*, 1973, **181**, 547–9.

18. A. J. Medford, A. Vojvodic, F. Studt, F. Abild-Pedersen, and J. K. Nørskov, *J. Catal.*, 2012, **290**, 108–117.

19. I. J. Hsu, D. A. Hansgen, B. E. McCandless, B. G. Willis, and J. G. Chen, *J. Phys. Chem. C*, 2011, **115**, 3709–3715.

20. D. V. Esposito, S. T. Hunt, Y. C. Kimmel, and J. G. Chen, *J. Am. Chem. Soc.*, 2012.

21. B. Hammer and J. K. Nørskov, *Nature*, 1995, **376**, 238–240.

22. M. Mavrikakis, B. Hammer, and J. K. Nørskov, *Phys. Rev. Lett.*, 1998, **81**, 2819–2822.

23. J. R. Kitchin, J. K. Nørskov, M. A. Barteau, and J. G. Chen, *Phys. Rev. Lett.*, 2004, **93**, 4–7.

24. J. R. Kitchin, J. K. Nørskov, M. A. Barteau, and J. G. Chen, *Catal. Today*, 2005, **105**, 66–73.

25. C. Ruberto, A. Vojvodic, and B. Lundqvist, *Surf. Sci.*, 2006, **600**, 1612–1618.

26. A. Vojvodic, C. Ruberto, and B. Lundqvist, *J. physics. Condens. matter*, 2010, **22**, 375504.

27. D. R. Lide, Ed., in *CRC Handbook of Chemistry and Physics*, CRC Press, Boca Raton, Florida, 84th edn., 2003, p. 76.

28. W. Lengauer, S. Binder, and K. Aigner, *J. Alloys Compd.*, 1995, **217**, 137–147.

29. L. Ramqvist, *Jernkontorets Ann.*, 1968, **152**, 465–475.

30. J. Leciejewicz, *Acta Crystallogr.*, 1961, **14**, 200–200.

31. Z. Li and R. Bradt, *J. Mater. Sci.*, 1986, **21**, 4366–4368.

32. E. Owen and E. Yates, *Philos. Mag. Ser. 7*, 1933, **15**, 472–488.

33. A. Vojvodic and C. Ruberto, *J. Phys. Condens. Matter*, 2010, **22**, 375501.

34. I. J. Hsu, Y. C. Kimmel, X. Jiang, B. G. Willis, and J. G. Chen, *Chem. Commun. (Camb).*, 2012, **48**, 1063–5.

35. S. Bağcı, S. Duman, H. M. Tütüncü, and G. P. Srivastava, *Diam. Relat. Mater.*, 2009, **18**, 1057–1060.

36. L. Vitos, A. V Ruban, H. L. Skriver, and J. Kolla, *Surf. Sci.*, 1998, **411**, 186–202.

37. L. S. Ramsdell, *Am. Minerol.*, 1947, **32**, 64.

38. H. O. Pierson, *Handbook of Refractory Carbides and Nitrides*, Noyes Publishers, Westwood, New Jersey, 1996.

39. R. F. W. Bader and P. M. Beddall, *Chem. Phys. Lett.*, 1971, **8**, 29–36.

40. F. Viñes, C. Sousa, P. Liu, J. A. Rodriguez, and F. Illas, *J. Chem. Phys.*, 2005, **122**, 174709.

41. R. S. Mulliken, *J. Chem. Phys.*, 1955, **23**, 1833.

42. Y. Li, Y. Gao, B. Xiao, T. Min, Z. Fan, S. Ma, and L. Xu, *J. Alloys Compd.*, 2010, **502**, 28–37.

43. W. J. Choyke, D. R. Hamilton, and L. Patrick, *Phys. Rev.*, 1964, **133**, 465.

44. A. Seidl, A. Görling, P. Vogl, J. A. Majewski, and M. Levy, *Phys. Rev. B. Condens. Matter*, 1996, **53**, 3764–3774.

45. S. Bahn and K. W. Jacobsen, *Comput. Sience Eng.*, 2002, **4**, 56–66.

46. S. Zaima, Y. Shibata, H. Adachi, and C. Oshima, *Surf. Sci.*, 1985, **157**, 380–392.

47. F. Bechstedt, P. Kackell, A. Zywietz, K. Karch, B. Adolph, K. Tenelsen, and J. Furthmuller, *Phys. Stat. Sol.*, 1997, **202**, 35–62.

48. D. J. Siegel, L. G. Hector, and J. B. Adams, *Surf. Sci.*, 2002, **498**, 21664–21671.

49. A. Vojvodic, A. Hellman, C. Ruberto, and B. Lundqvist, *Phys. Rev. Lett.*, 2009, **103**, 1–4.

50. J. Yates and G. Jones, *Unpublished work*, .

51. J. Meier, J. Schiøtz, P. Liu, J. K. Nørskov, and U. Stimming, *Chem. Phys. Lett.*, 2004, **390**, 440–444.

52. F. Abild-Pedersen, J. Greeley, F. Studt, J. Rossmeisl, T. Munter, P. Moses, E. Skúlason, T. Bligaard, and J. Nørskov, *Phys. Rev. Lett.*, 2007, **99**, 016105.

53. E. M. Fernández, P. G. Moses, A. Toftelund, H. a Hansen, J. I. Martínez, F. Abild-Pedersen, J. Kleis, B. Hinnemann, J. Rossmeisl, T. Bligaard, and J. K. Nørskov, *Angew. Chem. Int. Ed. Engl.*, 2008, **47**, 4683–6.

54. J. K. Nørskov, F. Abild-Pedersen, F. Studt, and T. Bligaard, *Proc. Natl. Acad. Sci. U. S. A.*, 2011, **108**, 937–43.

55. S. Clark and M. Segall, *Zeitschrift für …*, 2005, **220**, 567–570.

56. D. Vanderbilt, *Appl. Opt.*, 1990, **41**, 7892.

57. J. Perdew, K. Burke, and M. Ernzerhof, *Phys. Rev. Lett.*, 1996, **77**, 3865–3868.

58. B. Hammer, L. B. Hansen, and J. K. Nørskov, *Phys. Rev. B*, 1999, **59**, 7413–7421.

59. H. Monkhorst and J. Pack, *Phys. Rev. B*, 1976, **13**, 5188–5192.

60. S. J. Jenkins, *Personal Communication*, .

61. A. Morris and C. Pickard, *LINDOS version 1.3 User Manual*, UCL, London, 2011.

62. H. Chhina, S. Campbell, and O. Kesler, *J. Power Sources*, 2007, **164**, 431–440.

63. M. Shao, B. Merzougui, K. Shoemaker, L. Stolar, L. Protsailo, Z. J. Mellinger, I. J. Hsu, and J. G. Chen, *J. Power Sources*, 2011, **196**, 7426–7434.

64. I. J. Hsu, Y. C. Kimmel, Y. Dai, S. Chen, and J. G. Chen, *J. Power Sources*, 2012, **199**, 46–52.